Photoelectron angular distributions of excited atoms in intense laser fields

C. H. Raymond Ooi,[1] WaiLoon Ho,[1] and A. D. Bandrauk[2]
[1]*Department of Physics, University of Malaya, 50603 Kuala Lumpur, Malaysia*
[2]*Laboratoire de Chimie Théorique, Faculté des Sciences, Université de Sherbrooke, Sherbrooke, Québec, J1K 2R1, Canada*
(Received 9 March 2014; published 17 July 2014)

Angular distributions of photoionization differential rates for an atom in arbitrary excited states ionized by intense laser fields with arbitrary polarization are reported. Relativistic effects are incorporated into the Keldysh theory, yielding semi-analytical expressions of ionization rates for hydrogenic initial states in intense linear, circular, and elliptical laser polarizations. Angular distributions are compared for different angular momentum quantum numbers, magnetic quantum numbers, and Keldysh parameters γ. The angular distributions are shown to depend strongly on γ, thus also reflecting the influence of relativistic effects. The sign of the magnetic quantum number, corresponding to different electron rotations, is shown to have a significant effect on photoelectron angular distributions in circularly polarized laser fields.

DOI: 10.1103/PhysRevA.90.013417 PACS number(s): 32.80.Rm, 33.80.Rv, 03.30.+p

I. INTRODUCTION

The study of intense laser-matter interactions and attosecond [1,2] physics over the past two decades has attracted significant attention. Advancement in the study of electron dynamics [3] in an intense laser is based on nonperturbative theory and involves understanding of the physical processes such as tunneling ionization (TI), multiphoton ionization (MPI) [4], above threshold ionization (ATI), and high harmonics generation (HHG) [5–9], etc.

The tunneling ionization concept by Corkum [4] provides classical description of the electron dynamics that forms the basis for understanding the high harmonic generation. The model was used to describe an electron in the strong electromagnetic fields, which first tunnels to the continuum and recollides with the parent ion, emitting a photon that has a maximum energy, $N_m\hbar\omega_0 = I_p + 3.17U_p$, where N_m is the number of incident photons. The ATI spectra depends on polarization, with circularly polarized pulses giving $2U_p$ of maximum energy [10]. Further extension by Lein incorporates recolliding electrons for molecular imaging [11,12] and spectroscopy [13], thus providing important applications for the development of intense light-matter interactions [14,15]. In the study of recollision processes with circular pulses, it is shown that there are a few rules of thumb which apply to systems more complex than atoms [16]. The analytical formula obtained for HHG [17] enhances the understanding of the nonperturbative strong-field processes. It is found that a static electric field can induce new effects such as dichroicism and ellipticity in HHG [18]. A scheme using a combination of HHG and a terahertz field to generate a single circularly polarized attosecond pulse was first proposed by Yuan and Bandrauk recently [19].

There have been efforts to generalize the Keldysh theory [20–22] to arbitrary internal states, such as the well-known Ammosov-Delone-Krainov (ADK) theory [23] that expressed the probability of tunneling ionization in an alternating field, of a complex atom and of an atomic ion. It is based on the result of Perelomov *et al.* [24]. Their works use the generalized asymptotic wave function to obtain the final photoionization rate for arbitrary values of n, l, and m in an electric field of arbitrary ellipticity, where n, l, and m are the principle, the orbital angular momentum, and azimuthal or magnetic quantum numbers, respectively. It is found that the ionization rate depends on the sign of m [25]. However, the calculation of the atomic ionization rate, which involves averaging the laser fields over one period of oscillation, is valid only in the low-frequency limit of the electromagnetic fields or TI regime, namely, $\omega \ll \omega_t$, where $\omega_t = 1/\tau_t$ and τ_t is the tunneling time, as is mentioned in the work of Keldysh.

The theory of Keldysh, despite being perturbative, has its appealing features, such as providing analytical expressions for certain cases of study. His adiabaticity parameter, $\gamma = \sqrt{I_p/2U_p}$, determines whether the photoionization is in the TI regime or the MPI regime, where I_p is the ionization potential of the atom and $U_p = e^2E^2/4m\omega^2$ is the ponderomotive energy. Typically, for high frequencies and weak fields or when the ponderomotive energy is lower than the ionization potential, the MPI process becomes dominant, where k number of photons are absorbed simultaneously during the transition from ground level to the continuum level. The tunneling ionization regime corresponds to the opposite case of high fields and low frequencies.

The Keldysh formalism [26] is valid only for small momenta, i.e., the terms higher than $p^2/\sqrt{2mI_p}$ are neglected. Our recent work provides an exact evaluation of the photoionization rate [27] for photoelectrons with arbitrary momentum using the Keldysh-type formalism that is perturbative and approximate. However, the theory is valid for hydrogenic atoms in the ground state only, and it is limited to the nonrelativistic regime. In view of the photoelectric effect, this means that when the photon energy far exceeds the ionization threshold, the photoelectron would be relativistic. The relativistic theory of photoionization has been used along with the R-matrix approach [28] but has not been adopted along with the Keldysh theory. Our work may be relevant to Milosevic *et al.*'s analytic tunnel ionization rates for hydrogenlike ions obtained using the semiclassical solution of the three-dimensional Dirac equation [29].

Here, we focus on the simple relativistic corrections to the Keldysh and strong-field approximation (SFA) theories, which neglects the intermediate levels involved in resonant or near-resonant transitions that may create coherent superpositions of bound states. This is justified for the following reasons. First, states above our initial excited states are completely ionized due to their smaller ionization potentials and therefore are

not contributing to Stark effects, etc. Second, states lower in energy, such as the ground state, will also be unimportant, as they are nonresonant in the dynamics because excited states have large ionization rates and small lifetimes. Third, we are considering ionizing laser with frequencies that are of resonant from any bound-bound transition or any excited state. Thus the main dynamics is described mainly by ionization, either by tunneling or above barrier ionization. An example of work that neglects the resonant transitions is that of Liu and Nisoli [30], where they considered the $2p$ excited state of He^+ treated in SFA approximation to study polarization of its harmonics in strong fields without concern for coupling to higher states nor ground states. Similarly, Frolov and co-workers considered an initial excited atom, namely, the p state, in obtaining the analytical formula for HHG with elliptically polarized laser fields [13].

In this paper, we present the generalization of the perturbative formalism to arbitrary initial excited states of a hydrogenic atom with relativistic kinetic energy and vectorial momentum of the photoelectron. Using semianalytical expressions, we compute and compare the angular distributions of the photoionization rate for linear and circular laser polarizations with arbitrary excited atomic states of different quantum numbers, n,l,m. This enables us to systematically study the effects of relativistic photoelectron and atomic polarization in excited states on photoionization. It is helpful not to underestimate our choice of hydrogenic atom, since the wave functions for the quantum states n,l,m are known analytically, the results can be interpreted more easily to provide clearer insights than using more complicated atoms or molecules. Likewise, actual energy levels with spin-orbit coupling and other relativistic interactions [31] can be included when precision is required. The relativistic photoionization rate is presented in Sec. II, and the matrix elements for the arbitrary excited state are calculated in Sec. III. The results are shown and discussed in Sec. IV.

II. PHOTOIONIZATION RATE FOR AN EXCITED ATOM

The photoionization is performed on an excited atom using a $\binom{\text{linear}}{\text{elliptical}}$ polarized intense laser field $\mathbf{E} = E\binom{\hat{z}\cos\omega t}{(\alpha\cos\omega t,\beta\sin\omega t,0)}$ and $\mathbf{E}\cdot\mathbf{r} = \binom{Er\cos\theta\cos\omega t}{Er\sin\theta C(t,\phi)}$, where $C(t,\phi) = \alpha\cos\omega t\cos\phi + \beta\sin\omega t\sin\phi$, with the coefficients α and β determining the ellipticity $\epsilon = \alpha/\beta$ of the laser field. The general photoionization rate (as shown in our previous result) is defined as

$$w = \frac{m}{(2\pi\hbar^2)^2}\int_0^{2\pi}\int_0^{\pi}\sum_{k=k_0}^{\infty}|L(\mathbf{p}_k)|^2 p_k\sin\Theta d\Theta d\Phi, \quad (1)$$

with the threshold index $k_0 = \frac{1}{\hbar}(I_n + U_p)$ and

$$\begin{aligned} L(\mathbf{p}_k) &= \frac{1}{2\pi}\int_{-T/2}^{T/2} V_0(\mathbf{\Pi}(t))e^{iS(\mathbf{p},t)}e^{-i(\Omega-k\omega)t}\omega dt \\ &= \frac{1}{2\pi}\int\frac{V_0(\mathbf{\Pi}_k(u))}{\sqrt{1-u^2}}e^{iS(\mathbf{p}_k,u)}du \\ &= \frac{1}{2\pi}\int_{-\pi}^{\pi} V_0(\Pi(s))\exp iS(\mathbf{p}_k,s)ds, \end{aligned} \quad (2)$$

with $u = \sin s$ and $s = \omega t$; $\Omega_n(p) = \frac{1}{\hbar}(K_0 + I_n + U_p)$; $I_n = I_0/n^2$ is the ionization energy from level n; $K_0 = c\sqrt{p^2+m^2c^2} - mc^2$ is the relativistic kinetic energy; and $U_p = c\langle\sqrt{(eA(t))^2+(mc)^2}\rangle - mc^2 = c\sqrt{\frac{1}{2}(eA)^2+(mc)^2} - mc^2$, with $A = E/\omega$ the relativistic ponderomotive energy [32], taken as the time average $\langle..\rangle$ of the term involving the vector potential $\mathbf{A}(t) = -\int_0^t \mathbf{E}(t')dt'$.

Here, $S(\mathbf{p},s)$ represents the action phase during the photoionization,

$$\begin{aligned} S(\mathbf{p},t) &= \frac{1}{\hbar}\int_0^t [I_n + K(\tau)]d\tau \\ &= \Omega_n(p)t + \frac{1}{\hbar}\int_0^t [K(\tau) - K_0 - U_p]d\tau, \end{aligned} \quad (3)$$

which is computed by numerical integration, since it is not possible to obtain an analytical expression.

For the nonrelativistic case, Eq. (3) reduces to

$$S(\mathbf{p},u) \to \frac{\Omega_n(p)\sin^{-1}u}{\omega} + \frac{1}{\hbar\omega}\begin{pmatrix} -\frac{eE}{m\omega}p_z(\sqrt{1-u^2}) - U_p u\sqrt{1-u^2} \\ -\frac{eE}{m\omega}\left[\frac{(\alpha+\alpha^*)}{2}p_x(\sqrt{1-u^2}) + \frac{(\beta+\beta^*)}{2}p_y u\right] - U_p(|\alpha|^2-|\beta|^2)u\sqrt{1-u^2}\end{pmatrix}, \quad (4)$$

where the arrow signifies the nonrelativistic limit.

Although we are studying the relativistic effects on the the photoionization, we may use the nonrelativistic Schrödinger equation and neglect corrections to the dipole approximation based on two recent reports. To first order the electron velocity $\mathbf{v}$ only depends on the electric field. According to Ref. [33], the second-order correction leads to a magnetic field $\mathbf{B} = \hat{e}\times\mathbf{E}/c$ and a ponderomotive gradient dU_p/dz. The first scales as $1/c$, whereas the gradient of U_p will be negligible for long-wavelength (adiabatic) pulses.

Klaiber *et al.* [34] showed that the magnetic correction is responsible for a momentum shift $I_p/3c$. Thus for excited states with small I_p this is negligible. Therefore in comparison to excited I_p, the ponderomotive energies will be much larger, thus necessitating a more accurate treatment.

We may use the nonrelativistic Schrödinger equation since the relativistic corrections are mainly causing the energy shift of bound levels such as the spin-orbit interactions, which introduce only a negligible quantitative effect on the photoionization process.

The relativistic corrections to the ponderomotive potential, despite being small, are more important than other relativistic corrections, because the ponderomotive potential appears in the phase factor or the action part S through the Volkov wave function that is sensitive to the photoionization time scale and

therefore would have significant impact on the behavior of photoionization.

The atom-light interaction is taken in the nonrelativistic dipole form $\mathbf{E}\cdot\mathbf{r}$ within dipole approximation. The spatial dependence of the electric field is neglected and contains only the time dependence $\sin(\omega t)$ or $\cos(\omega t)$, as we assume the wavelength of interest is not too short but longer than a hard x ray or γ ray and much larger than the atomic dimension of 0.1 nm.

The transition matrix element $V_0(\mathbf{\Pi}(x))$ corresponds to the transition of the photoelectron from the initial state $\psi_s(\mathbf{r})$ to the continuum Volkov state $\psi_p(\mathbf{r},t)=\exp\{\frac{i}{\hbar}[\mathbf{\Pi}(t)\cdot\mathbf{r}-\int_0^t K(\tau)d\tau]\}$, with $\mathbf{\Pi}(t)=m\mathbf{v}=\mathbf{p}+e\mathbf{A}(t)$, and $K(\tau)=c\sqrt{\Pi(\tau)^2+m^2c^2}-mc^2\rightarrow\frac{\Pi(\tau)^2}{2m}$, i.e.,

$$V_0(t)=eE\iiint\psi_s(\mathbf{r})r\begin{pmatrix}\cos\theta\cos\omega t\\ F(t,\phi)\sin\theta\end{pmatrix}e^{-i\Xi}r^2drd\Omega, \quad (5)$$

where $d\Omega=\sin\theta d\theta d\phi$ and

$$F(t,\phi)=(\alpha\cos\omega t\cos\phi+\beta\sin\omega t\sin\phi), \quad (6)$$

$$\Xi(r,\theta,\phi,t)=\frac{1}{\hbar}\mathbf{\Pi}(t)\cdot\mathbf{r}=B(\theta,\phi,t)r, \quad (7)$$

$$B(\theta,\phi,t)=\frac{1}{\hbar}[Q(\phi,t)\sin\theta+P(t)\cos\theta], \quad (8)$$

with the integration over the radial part that consists of

$$P=\begin{pmatrix}p_z-e\frac{E}{\omega}\sin\omega t\\ p_z\end{pmatrix}, \quad (9)$$

$$Q=\begin{pmatrix}p_x\cos\phi+p_y\sin\phi\\ (p_x-\frac{eE}{\omega}\alpha\sin\omega t)\cos\phi+(p_y+\frac{eE}{\omega}\beta\cos\omega t)\sin\phi\end{pmatrix}. \quad (10)$$

However, the angular dependence of the photoionization rate is obtained by differentiating Eq. (1) with respect to the polar angle Θ and the azimuthal angle Φ:

$$\frac{dw}{d\Omega_a}=\frac{m}{(2\pi\hbar^2)^2}\sum_{k=k_0}^{\infty}|L(\mathbf{p}_k)|^2p_k. \quad (11)$$

III. TRANSITION MATRIX ELEMENT FOR ARBITRARY INITIAL STATE

Here, we focus the study on how the angular distribution depends on an individual initial state (a particular nlm) first before exploring the more elaborate situations of atomic gas in many excited states. Atomic gas in a single excited state can be realized by preparing the atoms predominantly in a single chosen excited state by the standard optical pumping technique by narrow-band lasers with certain polarizations, as used for atomic spectroscopy and laser cooling [35]. We illustrate this realization in Fig. 1. Photoionization with atoms in initial excited state has been studied by Bauer [36], who found additional peaks in the photoelectron spectra for the initial state in $n=2$ but neglected the magnetic quantum number m.

The general hydrogen wave function is considered, $\psi_s(\mathbf{r})=\psi_{n,l,m}(\mathbf{r})=R_{nl}(\mathbf{r})Y_l^m(\theta,\phi)$, with normalization $\int|\psi_0(\mathbf{r})|^2d^3r=1$. The radial wave function defined

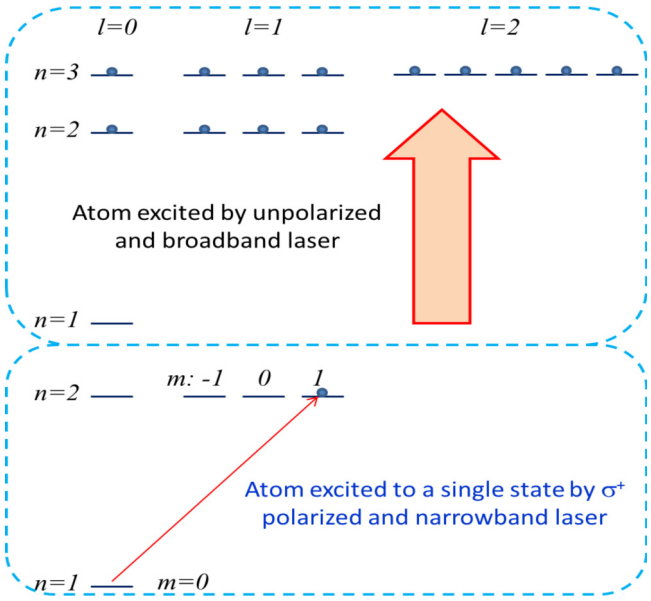

FIG. 1. (Color online) Atomic scheme showing atoms initially prepared in several internal states (top panel) and a particular state (bottom) before photoionization.

as $R_{nl}=\sqrt{(2\rho)^3\frac{(n-l-1)!}{2n[(n+l)!]^3}}e^{-\rho r}(2\rho r)^l[L_{n-l-1}^{2l+1}(2\rho r)]$ with $\rho=\frac{4\pi^2\mu e^2Z}{nh^2}=\frac{Z}{na_0}$, and the angular wave function is defined as $Y_l^m(\theta,\phi)=\sigma\sqrt{\frac{(2l+1)}{4\pi}\frac{(l-|m|)!}{(l+|m|)!}}e^{im\phi}P_l^m(\cos\theta)$, where $L_n^{(a)}(x)=\sum_{j=0}^n(-1)^j\binom{n+a}{n-j}\frac{x^j}{j!}$ is the associated Laguerre polynomials, $\sigma=\{\begin{smallmatrix}(-1)^m\text{ if }m\geqslant0\\ 1\text{ if }m<0\end{smallmatrix}\}$ is the piecewise function, $P_l^m(x)=\frac{(-1)^m}{2^ll!}(1-x^2)^{m/2}\frac{d^{l+m}}{dx^{l+m}}(x^2-1)^l$ is the associated Legendre polynomials.

Hence the transition matrix element of the initial state of the arbitrary energy level to the continuum Volkov state is redefined as

$$V_0(\mathbf{p})=\int\psi_s(\mathbf{r})e\mathbf{E}\cdot\mathbf{r}\exp\left(-\frac{i}{\hbar}\mathbf{p}\cdot\mathbf{r}\right)d^3r=e\mathbf{E}\cdot i\hbar\nabla_{\mathbf{p}}\tilde{\psi}_s(\mathbf{p}). \quad (12)$$

The goal of evaluating the matrix element $V_0(\mathbf{\Pi}(t))$ can be done by direct integration:

$$V_0(\Pi)=\int_0^\infty\int_0^\pi\int_0^{2\pi}e^{-i\Xi}e\mathbf{E}\cdot\mathbf{r}\psi_{n,l,m}(\mathbf{r})r^2drd\Omega$$
$$=A_{nlm}\int_0^\pi\int_0^{2\pi}Z_{nlm}(t,\theta,\phi)d\phi d\theta, \quad (13)$$

$$Z_{nlm}(t,\theta,\phi)=W_{nl}(t,\theta,\phi)C_{lm}(t,\theta,\phi), \quad (14)$$

with the coefficient factor varying with the different nlm,

$$A_{nlm}=\left(\frac{na_0}{2}\right)^{5/2}eE\sigma\sqrt{\frac{(n-l-1)!}{2n[(n+l)!]^3}\frac{(2l+1)}{4\pi}\frac{(l-|m|)!}{(l+|m|)!}}, \quad (15)$$

and the function that depends on time and angles θ, ϕ,

$$C_{lm}(t,\theta,\phi)=\begin{pmatrix}\cos\omega t\cos\theta\\ F(t,\phi)\sin\theta\end{pmatrix}P_l^m(\cos\theta)e^{im\phi}\sin\theta. \quad (16)$$

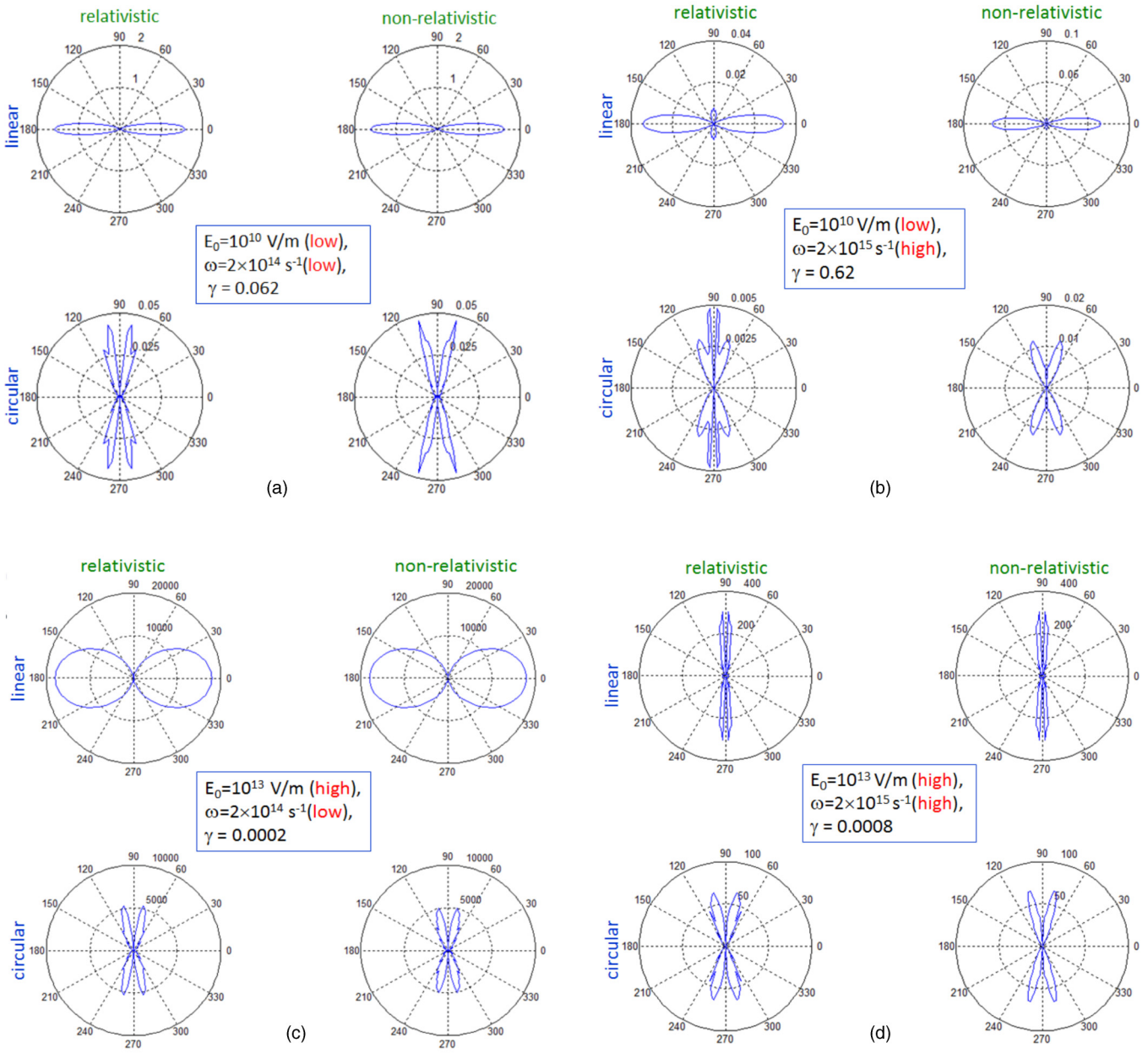

FIG. 2. (Color online) Angular distribution of photoionization rate from relativistic (left) and nonrelativistic (right) results for linear and circular polarizations on atom in state $n,l,m = 3,0,0$. The plots are shown for large and small combinations of E_0 and ω.

The integration over r can be rewritten in dimensionless quantities $x = 2r/na_0$ and $q = (iBa_0n + 1)/2$ as

$$W_{nl}(t,\theta,\phi) = \int_0^\infty x^{l+3} L_{n-l-1}^{2l+1}(x) \exp[-qx]dx. \qquad (17)$$

Using the identity $\int_0^\infty e^{-sx} x^\beta L_m^\alpha(x)dx = \frac{\Gamma(\beta+1)\Gamma(\alpha+m+1)}{m!\Gamma(\alpha+1)} s^{-(\beta+1)} F(-m,\beta+1;\alpha+1;\frac{1}{s})$, we have the exact expression

$$W_{nl}(t,\theta,\phi) = \mathcal{W}_{nl} q^{-(l+4)} F\left[-(n-l-1),l+4;2l+2;\frac{1}{q}\right], \qquad (18)$$

where $\mathcal{W}_{nl} = \frac{\Gamma(l+4)\Gamma(l+1+n)}{(n-l-1)!\Gamma(2l+2)}$.

For linear polarization the integration over ϕ has the form $\int_0^{2\pi} \exp[-i\frac{1}{\hbar}(p_x\cos\phi + p_y\sin\phi)\sin\theta r]e^{im\phi}d\phi$, while for elliptical polarization, $\int_0^{2\pi} (\sin\phi \text{ or } \cos\phi)\exp[A\cos\phi + B\sin\phi]e^{im\phi}d\phi$. If we neglect p_x and p_y for linear polarization, the matrix element is finite only for $m = 0$ since $\int_0^{2\pi} e^{im\phi}d\phi = 2\pi\delta_{m,0}$. This gives

$$V_0(\Pi(t)) = 2\pi A_{nl0}\cos\omega t \int_0^\pi W_{nl}(t,\theta)C_{l0}(t,\theta)d\theta, \qquad (19)$$

where $A_{nl0} = (\frac{na_0}{2})^4 eE\sqrt{(\frac{2}{na_0})^3 \frac{(n-l-1)!}{2n[(n+l)!]^3}\frac{(2l+1)}{4\pi}}$.

For $nlm = n00$ the integration over r becomes

$$W(t,\theta,\phi) = \frac{\Gamma(4)\Gamma(n+1)}{(n-1)!\Gamma(2)} q^{-4} F\left(1-n,4;2;\frac{1}{q}\right)$$

$$= 32n[3n^2(iBa_0-1)^2 + 1 - n^2]\frac{\Lambda_-^{n-3}}{\Lambda_+^{n+3}}, \qquad (20)$$

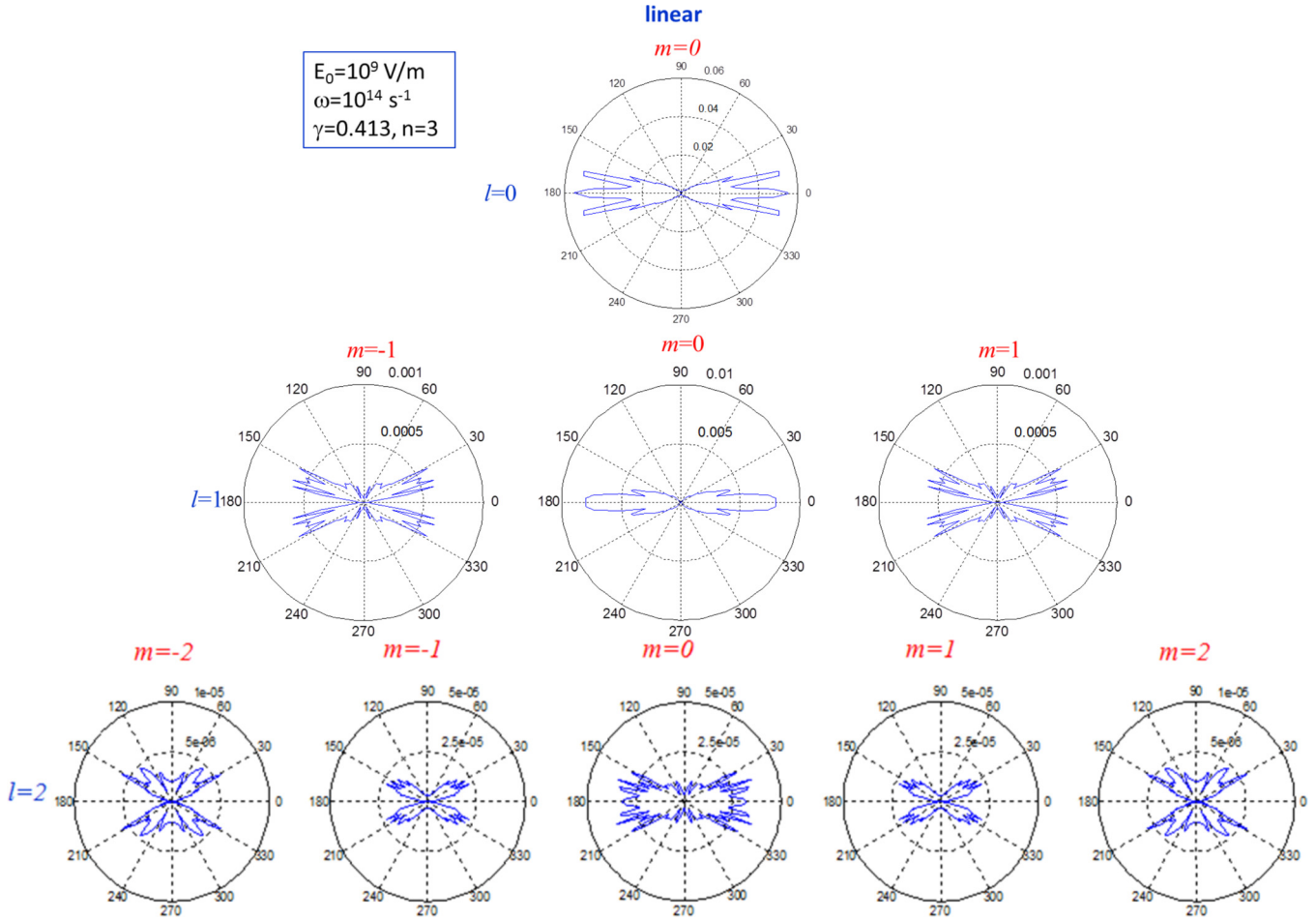

FIG. 3. (Color online) Angular distribution of photoionization rate for linear polarization with different initial excited atomic states in level $n = 3$.

where $\Lambda_\pm = (iBa_0n \pm 1)/2$, with $P_0^0(\cos\theta) = 1$ and $A_{n00} = (\frac{na_0}{2})^4 eE_0\sqrt{\frac{1}{4\pi}(\frac{2}{na_0})^3\frac{(n-1)!}{2n[(n+l)!]^3}}$. For state $|n00\rangle$ the results of Eq. (18) correspond exactly with Eq. (20).

For $n = 1$ and linear polarization, $B = \frac{1}{\hbar}[(p_x\cos\phi + p_y\sin\phi)\sin\theta + (p_z + e\frac{E}{\omega}\sin\omega t)\cos\theta]$. So far in many existing works and our previous work, p_x and p_y were neglected, so there was no dependency on ϕ and we recover the known result $V_0(\mathbf{\Pi}(t)) = 64\pi A_{nlm}3\cos\omega t\int_0^\pi \frac{\cos\theta\sin\theta d\theta}{(iBa+1)^4} = -i2\pi(2a_0)^4 eE\sqrt{\frac{1}{\pi a_0^3}\frac{\frac{a_0P_z}{\hbar}\cos\omega t}{[1+(\frac{a_0P_z}{\hbar})^2]^3}}$. Thus our present formalism is generalized to include the transverse momentum p_x and p_y. Hence the ϕ integration is present and has to be done numerically.

The matrix element for general nlm is evaluated from a semianalytical expression through numerical integrations over θ and ϕ:

$$V_0(\mathbf{\Pi}(t)) = -B_{nlm}\int_0^{2\pi}\int_0^{\pi} q^{-(l+4)}F\left(l+1-n,l+4;2l+2;\frac{1}{q}\right)\begin{pmatrix}\cos\omega t\cos\theta\sin\theta\\ F(t,\phi)\sin^2\theta\end{pmatrix}P_l^m(\cos\theta)e^{im\phi}d\theta d\phi, \quad (21)$$

where $B_{nlm} = A_{nlm}W_{nl}$. The integration over ϕ has to be done numerically due to the dependence on ϕ in B or finite values of p_x and p_y. Equation (21) is a general semianalytical formula, convenient for computing the photoionization rate versus angle of observation Θ for different initial states. It is valid for both linear and elliptical polarizations.

IV. RESULTS AND DISCUSSION

We have plotted the angular distributions of the differential photoionization rate $dw/d\Theta d\Phi = \frac{m}{(2\pi\hbar^2)^2}\sum_{k=k_0}^{\infty}|L(\mathbf{p}_k)|^2 p_k\sin\Theta$ using Eq. (1) at $\Phi = 0$ for linear and circular polarizations with relativistic and nonrelativistic results in Fig. 2. The $L(\mathbf{p}_k)$ is calculated using Eq. (2), which contains the action S given by Eq. (3) and V_0 given by Eq. (21). (Typically, figures are reported in V/cm for electric fields E and s^{-1} for frequencies for which $E(1\text{a.u.}) = 5.14\times10^9$ V/cm, $\omega(1\text{a.u.}) = 2\pi f = 4\times10^{16}$ s^{-1}) [37].

The four scenarios of high or low E and ω for $n,l,m = 3,0,0$ show that the relativistic and nonrelativistic results agree very well only for a sufficiently small relativistic Keldysh parameter

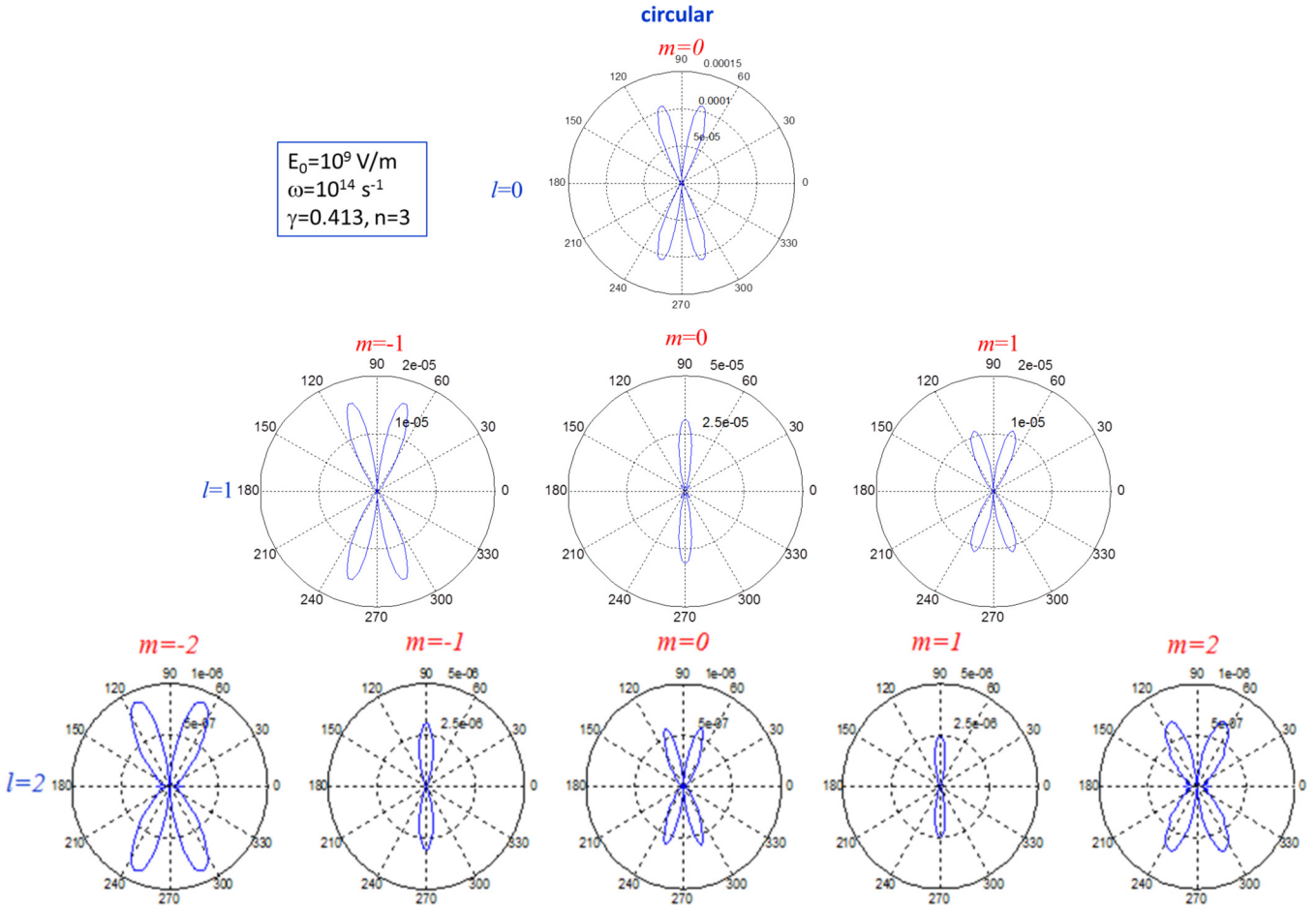

FIG. 4. (Color online) Angular distribution of photoionization rate for circular polarization with different initial excited atomic states in level $n = 3$.

$\gamma = \sqrt{I_p/2U_p} \approx \frac{\omega}{E}\sqrt{\frac{2mI_p}{e^2}}$, as in the case Fig. 2(c), where the fields are strong at low frequencies. At high frequencies and even with low fields, the relativistic effect is significant, as clearly shown in Fig. 2(b). This also provides good results on the relativistic photoelectric effect, where larger photon energy translates to a photoelectron with higher speed. Thus in the case of larger γ, the photoelectron emission probability is much smaller than in the nonrelativistic case and the case of small γ.

Let us analyze the angular distributions of photoelectrons from different orbitals in the excited states. For linear polarization (Fig. 3), the angular distributions do not depend on the sign of the magnetic quantum number m. For circular polarization (Fig. 4), the emission profiles are different for $+|m|$ and $-|m|$, although the shape looks identical, for $\gamma \simeq 0.4$ (<1). For $\gamma > 1$, however, the shapes are different for positive and negative m, such as additional more rounded lobes for positive m, connected to recent results [25]. In general, the lobes for linear polarization are almost complementary to the lobes for circular polarization, i.e., the minimum in the linear case corresponds to the maximum in the circular case, and vice versa. For linear polarization with $m = 0, \pm 2$ the photoelectron emission rate is the highest mainly at around $\Theta = \pi/2$ and it reduces with l. For $m = \pm 1$, there is zero emission towards $\Theta = \pi/2$. This result is counterintuitive, as one would expect that a higher excited state would be more likely to be ionized and the electron is ejected predominantly along $\Theta = 0$. For circular polarization (Fig. 4) with $m = 0$, the emission is highly directional with twin peaks close to $\Theta = \pi/2$.

Now we look at the angular distributions in excited states for different values of the Keldysh parameter γ. We plotted the angular distributions of spherically symmetric states $|n00\rangle$ with $n = 1$–4 in Figs. 5 and 6 for linear and circular polarizations, respectively. For $\gamma \gg 1$, the multiphoton ionization regime, the photoelectron emission basically follows the direction of the linear polarized electric field and close to the field direction of the circularly polarized light, especially for higher excited levels where the ionization energies are smaller. For $\gamma \sim 1$ the photoelectron can be emitted into several other directions, especially for lower levels. For $\gamma \ll 1$, the tunnel ionization regime, the photoelectron is emitted into multiple discrete directions as in Ref. [38], and it becomes hard to distinguish the angular distributions between linear and circular polarized lights. The increased isotropy in the emission reflects the nature of the tunneling process, which is probabilistic.

The general trend shown in Figs. 5 and 6 is that the emission rates are typically much larger for linear polarization and the rates increase with the electric field. But the angular

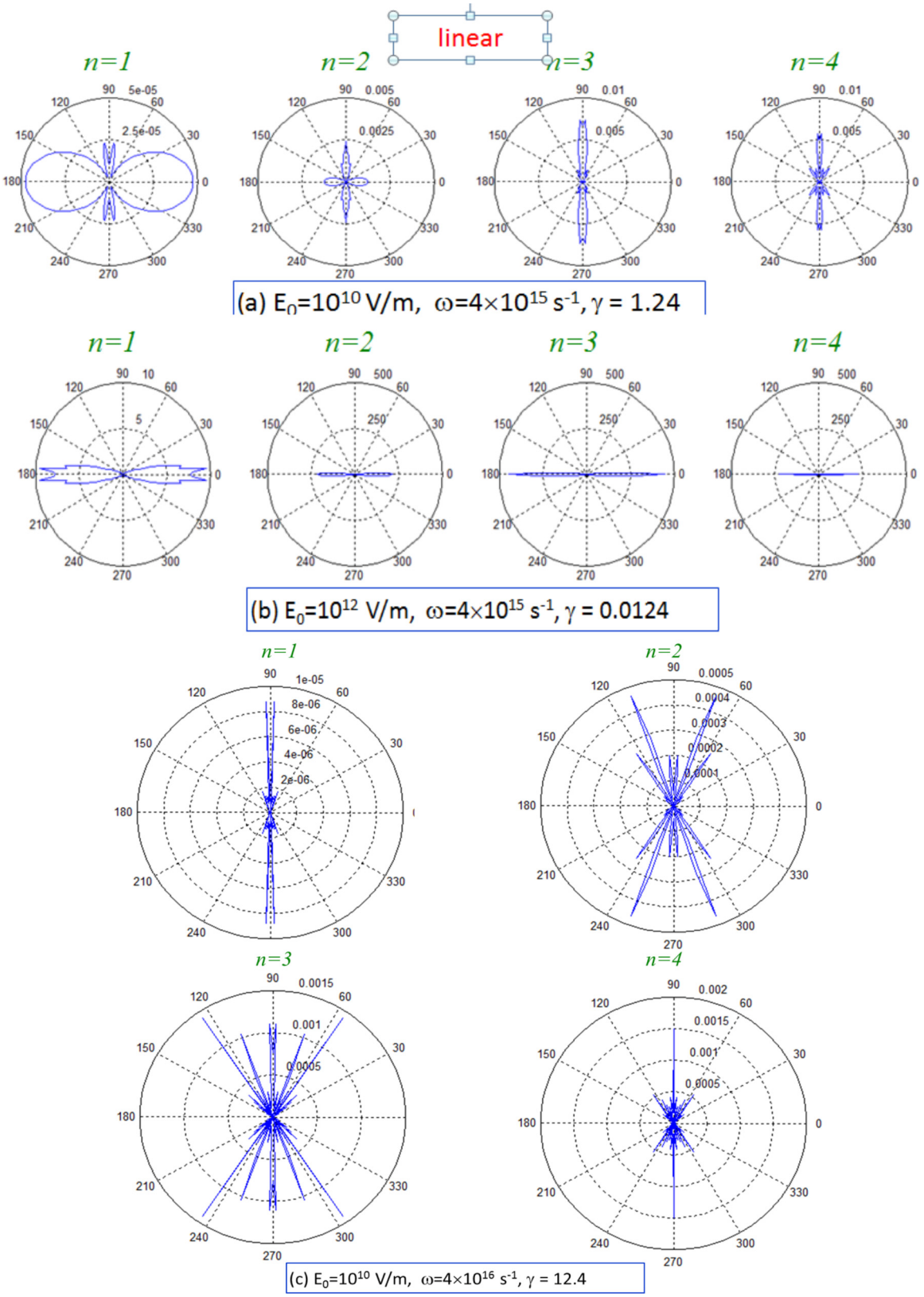

FIG. 5. (Color online) Angular distribution of photoionization rate for linear polarization of the first four states $|nlm\rangle = |n00\rangle$ ($n = 1,2...4$) with: (a) $\gamma \sim 1$ (b) $\gamma \ll 1$ (c) $\gamma \gg 1$.

distributions do not change significantly with the electric field strength. The photoionization rate increases with the initial state n up to $n = 3$ and then reduces for larger n. The shape is cosΘ-like for the linear case and sinΘ -like for the circular polarization corresponding to unidirectional, and bidirectional close to $\Theta = \pi/2 \pm \epsilon$, where ϵ is a small positive value.

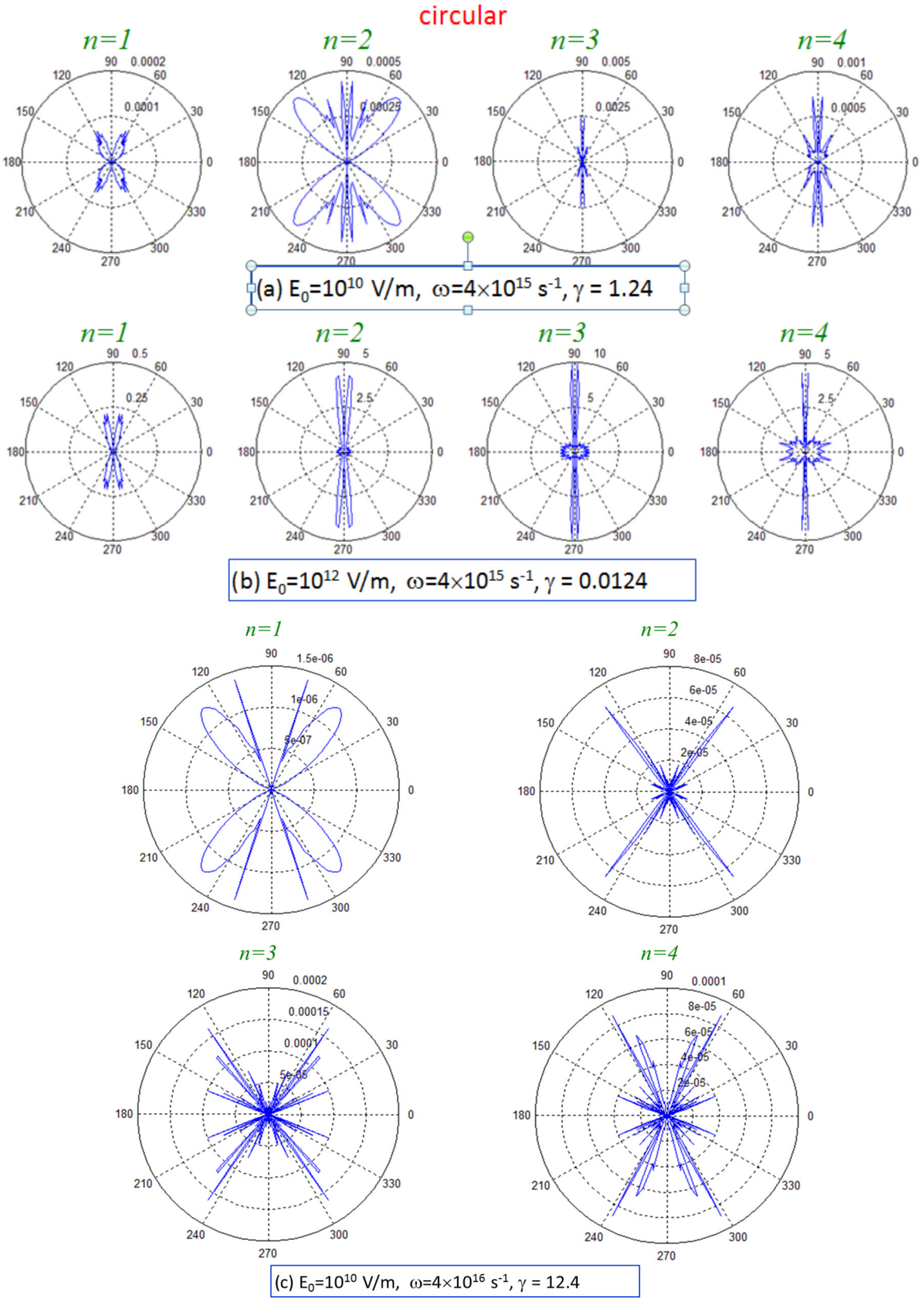

FIG. 6. (Color online) Angular distribution of photoionization rate for circular polarization of the first four states $|nlm\rangle = |n00\rangle$ ($n = 1,2...4$) with: (a) $\gamma \sim 1$ (b) $\gamma \ll 1$ (c) $\gamma \gg 1$.

In regular atomic gas the atoms are in more than one initial state. We may consider the initial superposition of states instead of a single quantum state, coupled by the intense laser with a power broadening effect or a broad bandwidth of the laser pulse. Then the initial atomic state becomes a superposition of all the angular momenta l and magnetic

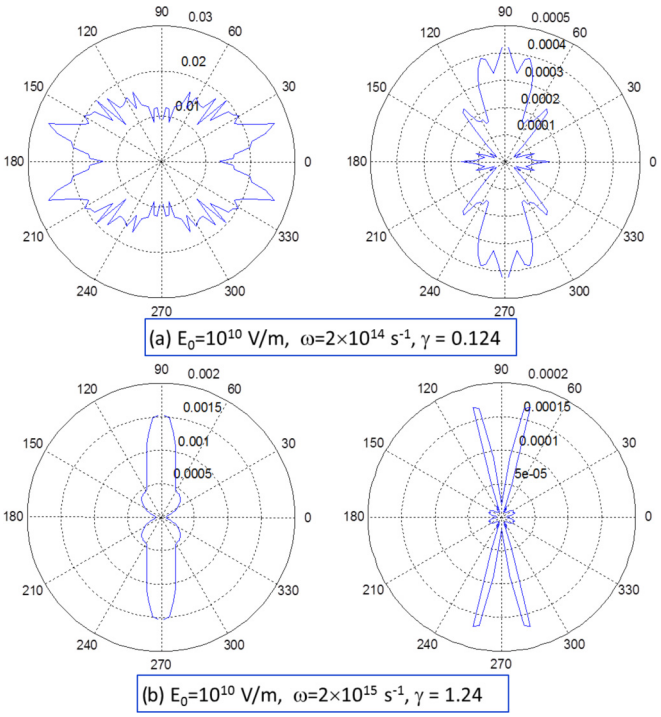

FIG. 7. (Color online) Angular distribution of photoionization rate for linear (left) and circular(right) polarizations for initial excited atom in $n = 2$, with superposition of states in $l = 0, m = 0$ and $l = 1$, $m = -1, 0, 1$.

substates m, i.e., $\psi_{n,l,m}(\mathbf{r})$ would be replaced by

$$\psi_n(\mathbf{r}) = \sum_{m=-l}^{l} \sum_{l=1}^{n-1} c_{nlm} \psi_{n,l,m}(\mathbf{r}), \tag{22}$$

where $\sum_{m=-l}^{l} \sum_{l=1}^{n-1} |c_{nlm}|^2 = 1$. The matrix element Eq. (13) becomes

$$V_0(\mathbf{\Pi}) = \sum_{m=-\boldsymbol{l}=1}^{l} \sum^{n-1} c_{nlm} A_{nlm} \int_0^{\pi} \int_0^{2\pi} Z_{nlm}(t, \theta, \phi)\, d\phi d\theta. \tag{23}$$

The eigenenergy that includes the effects of fine-structure interaction is given by $E_{nj} = -|I_n|[1 + (\frac{Z\alpha}{2n})^2 (\frac{4n}{j+1/2} - 3)]$, where $I_n = -\frac{Z^2}{n^2} I_0$, $I_0 = hcR_\infty = \frac{\alpha^2 m_e c^2}{2} = 13.6$ eV, and $|l - \frac{1}{2}| \leq j \leq l + \frac{1}{2}$. Except for spectroscopic purposes, the spin-orbit splitting can be neglected and we just use $E_{nj} \simeq -\frac{Z^2}{n^2} 13.6$ eV for all states within the same n.

To show the effects of superposition of states and independent sum of probabilities of those states, we perform simulations for $n = 2$ with $l = 0, m = 0$ and $l = 1, m = -1, 0, 1$. Figure 7 shows that the angular distribution assumes a more rounded shape, combining the features of all the magnetic substates. For circular polarization, the X-shape distribution in Fig. 7(b) from $m = \pm 1$ is so strong that it stands out of the superposition with the $m = 0$. However, typically information from the substates cannot be extracted effectively when the initial state is composed of many states. Therefore more useful information can be obtained if the atoms are prepared in a single m state, corresponding to left or right rotation, as shown in [25], which enables the study of how photoionization depends on the angular momentum and its magnetic substates.

V. CONCLUSIONS

We have shown from simulations using the semianalytical Keldysh theory, including relativistic corrections to the ponderomotive energy [21], that relativistic corrections become more significant for a larger Keldysh parameter γ, characteristic of the MPI regime. In the case of large γ and n, photoelectrons can be emitted into many discrete directions, with no simple angular distribution. The results also show that photoelectron angular distribution is sensitive to the magnetic quantum number m, which enables us to distinguish the state of a degenerate atom in different internal magnetic states. This could be a useful tool to identify the polarization of the atom by the angular distribution of the photoelectron in the absence of magnetic fields, since the different magnetic states cannot be distinguished by spectroscopic data. Circular and elliptic polarizations are new tools in studying the tunneling and MPI regimes in intense laser fields, but these have neglected relativistic effects which we show can be important since they modify the ponderomotive energies.

Our results show that relativistic corrections to ponderomotive energies, which cause the large energy shifts of excited states, leads to important physical effects in strong-field physics of atoms. This shows that corrections to the strong-field approximation (SFA) models are already necessary for excited states. Our work points to a new direction in strong-field physics which needs to be verified next by exact calculations as well as experiments.

ACKNOWLEDGMENT

This work is supported by High Impact Research, Grant No. UM.C/625/1/HIR/MOHE/CHAN/04, from the Ministry of Education of Malaysia.

[1] F. Krausz and M. Ivanov, Rev. Mod. Phys. **81**, 163 (2009).
[2] P. B. Corkum and F. Krausz, Nat. Phys. **3**, 381 (2007).
[3] S. Baker *et al.*, Science **312**, 424 (2006).
[4] P. B. Corkum, Phys. Rev. Lett. **71**, 1994 (1993).
[5] M. Lewenstein, Ph. Balcou, M. Y. Ivanov, A. L'Huillier, and P. B. Corkum, Phys. Rev. A **49**, 2117 (1994).
[6] K. J. Yuan and A. D. Bandrauk, Phys. Rev. A **81**, 063412 (2010).
[7] R. Baer, D. Neuhauser, P. R. Ždánská, and N. Moiseyev, Phys. Rev. A **68**, 043406 (2003).
[8] O. Smirnova, S. Patchkovskii, Y. Mairesse, N. Dudovich, D. Villeneuve, P. Corkum, and M. Y. Ivanov, Phys. Rev. Lett. **102**, 063601 (2009).

[9] K. J. Yuan and A. D. Bandrauk, J. Phys. B: At., Mol. Opt. Phys. **45**, 074001 (2012).
[10] P. B. Corkum, N. H. Burnett, and F. Brunel, Phys. Rev. Lett. **62**, 1259 (1989).
[11] M. Lein, J. Phys. B **40**, R135 (2007).
[12] N. Milosevic, P. B. Corkum, and T. Brabec, Phys. Rev. Lett. **92**, 013002 (2004).
[13] M. V. Frolov, N. L. Manakov, T. S. Sarantseva, and A. F. Starace, Phys. Rev. A **86**, 063406 (2012).
[14] M. Protopapas, D. G. Lappas, and P. L. Knight, Phys. Rev. Lett. **79**, 4550 (1997).
[15] E. Lorin, S. Chelkowski, and A. Bandrauk, Comput. Phys. Commun. **177**, 908 (2007).
[16] A. Kamor, F. Mauger, C. Chandre, and T. Uzer, Phys. Rev. Lett. **110**, 253002 (2013).
[17] M. V. Frolov, N. L. Manakov, T. S. Sarantseva, M. Yu. Emelin, M. Yu. Ryabikin, and A. F. Starace, Phys. Rev. Lett. **102**, 243901 (2009).
[18] B. Borca, A. V. Flegel, M. V. Frolov, N. L. Manakov, D. B. Milošević, and A. F. Starace, Phys. Rev. Lett. **85**, 732 (2000).
[19] K.-J. Yuan and A. D. Bandrauk, Phys. Rev. Lett. **110**, 023003 (2013).
[20] K. Mishima, M. Hayashi, J. Yi, S. H. Lin, H. L. Selzle, and E. W. Schlag, Phys. Rev. A **66**, 033401 (2002).
[21] V. N. Ostrovsky, T. K. Kjeldsen, and L. B. Madsen, Phys. Rev. A **75**, 027401 (2007).
[22] H. Mineo, S. D. Chao, K. Mishima, K. Nagaya, M. Hayashi, and S. H. Lin, Phys. Rev. A **75**, 027402 (2007).
[23] M. V. Ammosov, N. B. Delone, and V. P. Krainov, Sov. Phys. JETP **64**, 1191 (1986).
[24] A. M. Perelomov, V. S. Popov, and M. V. Terent'ev, Sov. Phys. JETP **23**, 924 (1966).
[25] T. Herath, L. Yan, S. K. Lee, and W. Li, Phys. Rev. Lett. **109**, 043004 (2012).
[26] L. V. Keldysh, Sov. Phys. JETP **20**, 1307 (1965) [Zh. Eksp. Teor. Fiz. **47**, 1945 (1964)].
[27] C. H. Raymond Ooi, W. L. Ho, and A. D. Bandrauk, Phys. Rev. A **86**, 023410 (2012).
[28] M. Gruchowski and R. Szmytkowski, Radiat. Phys. Chem. **68**, 143 (2003).
[29] N. Milosevic, V. P. Krainov, and T. Brabec, Phys. Rev. Lett. **89**, 193001 (2002).
[30] C. Liu and M. Nisoli, Phys. Rev. A **85**, 013418 (2012).
[31] S. T. Manson and A. F. Starace, Rev. Mod. Phys. **54**, 389 (1982).
[32] G. A. Mourou, T. Tajima, and S. V. Bulanov, Rev. Mod. Phys. **78**, 309 (2006).
[33] C. T. L. Smeenk, L. Arissian, B. Zhou, A. Mysyrowicz, D. M. Villeneuve, A. Staudte, and P. B. Corkum, Phys. Rev. Lett. **106**, 193002 (2011).
[34] M. Klaiber, E. Yakaboylu, H. Bauke, K. Z. Hatsagortsyan, and C. H. Keitel, Phys. Rev. Lett. **110**, 153004 (2013).
[35] C. E. Wieman, D. E. Pritchard, and D. J. Wineland, Rev. Mod. Phys. **71**, S253 (1999).
[36] J. H. Bauer, Phys. Rev. A **85**, 063417 (2012).
[37] In one atomic units (1 a.u.), the energy is 27.2 eV $= 2I_p(1s)$ corresponding to wavelength $\lambda = 45$ nm, frequency $f = 6.58 \times 10^{15}$ s^{-1}, and angular frequency $\omega = 2\pi f = 4 \times 10^{16}$ s^{-1}. The electric field is $E_0(1s) = 5.14 \times 10^9$ V/cm, corresponding to intensity $I_0 = 3.5 \times 10^{16}$ W/cm^2.
[38] Z. Zhou and Shih-I. Chu, Phys. Rev. A **83**, 033406 (2011).